IEEE Access
Multidisciplinary ⋮ Rapid Review ⋮ Open Access Journal

Received June 29, 2020, accepted July 15, 2020, date of publication July 28, 2020, date of current version August 17, 2020.

Digital Object Identifier 10.1109/ACCESS.2020.3012510

Reduced Reference Frame Transform: Deconstructing Three-Phase Four-Wire Systems

FRANCISCO CASADO-MACHADO, (Graduate Student Member, IEEE), JOSE L. MARTINEZ-RAMOS, (Senior Member, IEEE), MANUEL BARRAGÁN-VILLAREJO, JOSÉ MARÍA MAZA-ORTEGA, (Member, IEEE), AND JOSÉ A. ROSENDO-MACÍAS, (Senior Member, IEEE)

Department of Electrical Engineering, University of Seville, 41092 Seville, Spain

Corresponding author: Francisco Casado-Machado (mfrancisco@us.es)

This work was supported by the Spanish Ministry of Economy and Competitiveness under Grant ENE2017-84813-R and it is part of the EASY-RES project that has received funding from the European Union's Horizon 2020 Research and Innovation program under Grant Agreement No. 764090.

ABSTRACT This paper proposes a new reference frame, namely Reduced Reference Frame (RRF), specially suited for unbalanced three–phase four–wire systems which improves the performance of the classical Fortescue, Clarke and Park transformations. The RRF transfomation allows to represent any unbalanced three–phase sinusoidal magnitude with just two components even if the zero–sequence component is present. For doing so, the RRF transformation takes into account that the *abc* space–vector trajectory of the transformed three–phase sinusoidal magnitude is always within a plane. The geometric properties of this trajectory are considered for outlining a general classification of the transformation depending on the input voltages and an adequate reference frame within the plane. Then, a step–by–step procedure for computing the transformation matrix is detailed. Once the voltages and currents are transformed into the RRF, it is proposed a power theory which allows to compute the instantaneous active and reactive powers. The paper includes two simulations and an experimental validation through a real–time application to highlight the benefits of the proposal. The paper closes with the main conclusions and some future research lines where this transformation can be applied.

INDEX TERMS Coordinate transformation, reference frame, three–phase four–wire systems, unbalanced power systems.

I. INTRODUCTION

Different transforms have been used in Electrical Engineering for analyzing, modelling and controlling power systems [1], electrical machines [2] or power electronic devices [3]. All of these transforms aim at turning the original formulation in the *abc* phase domain into an alternative domain where a simple model is obtained.

C.L. Fortescue presented a transform for the steady–state analysis of unbalanced three–phase systems [4]. In this case, the original unbalance problem is transformed to three balanced systems, namely: positive, negative and zero sequence systems. By doing so, it is not required to resort to a phase–coupled three–phase analysis of the original unbalanced system. Instead, the problem can be solved by a single–phase formulation where the different sequence systems are involved. For this reason, the Fortescue's transform is widely used for the computation of unbalanced short-circuit faults, e.g. ground–to–line or line–to–line faults [5], in power systems.

R.H. Park proposed a transformation from *abc* to *dq0* reference frame for modelling rotating electrical machines in dynamic conditions [6]. This *dq0* reference frame rotates synchronously with the system frequency which notably simplifies the machine analysis because of two reasons. On the one hand, the magnetic coupling between rotor and stator is no longer dependent on the angular position which significantly reduces the simulation computational cost [2]. On the other hand, and due to the fact that rotating electrical machines are three–phase three–wire systems, it is possible to reduce the analysis to just *d* and *q* magnitudes in case of balanced supply conditions, being null the *0* magnitude.

E. Clarke proposed a transformation to the so-called $\alpha\beta 0$ stationary reference frame rather than the Park rotating

The associate editor coordinating the review of this manuscript and approving it for publication was Kan Liu.

one [7]. In this case, a balanced set of three-phase sinusoidal *abc* magnitudes are transformed into two orthogonal sinusoidal magnitudes in the $\alpha\beta$ axes with equal amplitude, being null the *0* component as in the case of the Park transformation.

In addition to these classical applications, the Park and Clarke transformations are widely used for controlling power electronic devices, from electrical drives [8] to grid–connected power converters [3]. Particularly, the Park transformation turns any set of balanced three–phase sinusoidal phase magnitudes into two constant values in the *dq* reference frame. In this way, the design of control strategies, such as Proportional Integral (PI) controllers, can be done in a straightforward manner by using classical control theory [9]. However, this requires the use of a synchronization system or Phase Lock Loop (PLL) [10] for estimating the frequency and the angle used in the transformation. On the other hand, the Clarke transformation had a revival in the eighties of the last century with the instantaneous reactive power theory proposed by Akagi *et al.* [11]. This elegant current computation technique allows to calculate the reactive power instantaneously with a clear application to static reactive power compensators. Moreover, its improvement for computing harmonic components gave rise to the development of active power filters [12]. In addition, the emergence of resonant controllers [13], able to assure a zero steady-state error tracking sinusoidal magnitudes, has boosted even more its use in the last years. These controllers prevent the use of PLLs, which is quite convenient in case of non-ideal voltages with a high imbalance and harmonic distortion content [14]. In these non-ideal conditions, it is highly recommended to use advanced PLLs with positive and negative sequence detectors to avoid power oscillations in three–phase three–wire systems [15].

Without any doubt, the usefulness of these transformations for three–phase and three–wire power electronic applications relies on the reduction from a three–component *abc* system to an equivalent one with just two components ($\alpha\beta$ or *dq*). This allows the application of complex algebra and the derivation of a solid power theory [16]. However, this advantage fades in case of three–phase and four–wire systems because it cannot be assured a null third *0* component after the application of the Park or Clarke transformation. In these situations, where the complex algebra cannot be longer applied, different power theories appeared [17]–[20], but all of them lacks of a solid mathematical foundation being just adaptations of the three–phase three–wire case. As a matter of fact, this is still an open question nowadays where new research dealing with these topics continuously arises [21]. G. Tan has proposed to transform the unbalanced magnitude into a non–orthogonal reference frame in such a way that this magnitude can be represented by means of a space vector of constant magnitude [22]. However, it can be only applied to three–phase three–wire systems. Other recently proposed transformations rely on techniques never applied before in this field such as mechanical approaches [23] or Singular Value Decomposition (SVD) [24], but with a high computational cost which prevents its use in real-time applications. Recently, A.A. Montanari and A.M. Gole propose a transformation to a new reference frame called *mno* to cope with three–phase four–wire systems including zero–sequence components and its corresponding power theory [25]. This formulation allows to relate different active and reactive power terms with the corresponding voltages and currents in the *mno* reference frame and, therefore, being suitable for the reference current computation of a static compensator. The differential characteristic of the Montanari transformation is the use of the voltage vector and its derivative in the reference frame definition rather than the angle used in the Park and Clarke transformations. However, it can be probed that this transformation is not defined for some particular voltage conditions, i.e. voltage with just zero-sequence component or null phase *a* voltage.

Following these later works, this paper proposes a stationary reference frame specially suited for three–phase and four–wire systems involving zero–sequence component named Reduced Reference Frame (RRF). This specific reference frame is based on the trajectory, or locus, defined by the space vector of the three–phase *abc* magnitude. This transformation allows to represent any three–phase *abc* magnitude just by two magnitudes or by one complex magnitude within the RRF. This complex magnitude in the RRF can be decomposed into two vectors rotating in opposite directions. This decomposition allows to classify the locus of the transformed magnitude generalizing its application for any three–phase *abc* magnitude. Once the RRF is defined, it is possible to formulate a power theory for computing the instantaneous active and reactive power. These power terms are considerably simplified if the voltage and current loci are within the same plane. In this case, a power definition similar to the one proposed by Akagi in [11] but including the zero sequence component is obtained.

The rest of the paper is organized as follows. Section II presents the fundamentals of the proposed RRF transformation including its definition, possible trajectories of the transformed magnitude and method for computing the transformation matrix. Section III formulates an instantaneous power theory in the RRF. Section IV applies the proposed RRF transformation to a case study with an unbalanced three–phase four–wire system for illustrative purposes. Section V details an experimental validation of the proposed RRF transformation to highlight its suitability for real-time applications. The paper closes with the main conclusions.

II. REDUCED REFERENCE FRAME

A. RRF FUNDAMENTALS

Let's consider a generic set of three-phase voltages formulated as:

$$v_i(t) = \sqrt{2}\, V_i \cos(\omega t + \theta_i) \quad i = a, b, c, \tag{1}$$

where i represents the phase of the system, ω is the angular frequency, V_i and θ_i are the RMS value and phase angle of the voltages respectively. This voltage may contain positive,

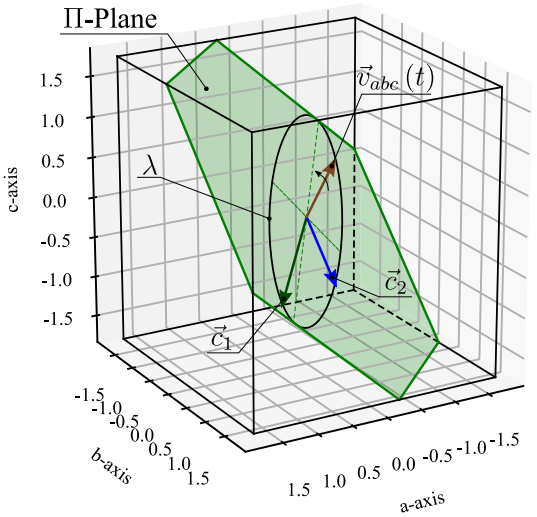

FIGURE 1. Representation of the voltage locus $\vec{v}_{abc}(t)$ within the Π–plane in *abc* coordinates.

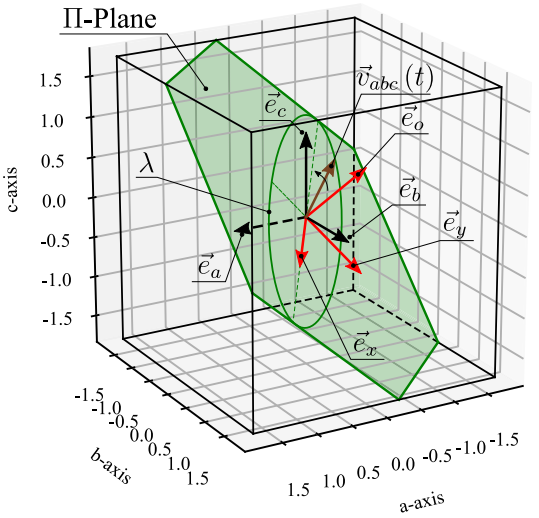

FIGURE 2. Representation of the Reduced Reference Frame (RRF) based on $\{\vec{e}_x, \vec{e}_y, \vec{e}_o\}$ within the Π–plane.

negative and zero sequence components as V_i and θ_i can take any value. These voltages can be represented as a space vector $\vec{v}_{abc}$ in an orthogonal *abc* space where each axis is associated to a phase angle voltage. In this way, the space vector $\vec{v}_{abc}$ describes a trajectory determined by [26], [27]:

$$\vec{v}_{abc}(t) = [v_a(t), v_b(t), v_c(t)]^T. \tag{2}$$

Each phase voltage v_i is the solution of a simple harmonic oscillator [28] defined by a homogeneous second order differential equation which can be extended to $\vec{v}_{abc}$ as:

$$\frac{d^2\vec{v}_{abc}}{dt^2} + \omega^2\vec{v}_{abc} = 0. \tag{3}$$

Consequently, the solution of (3) can be expressed as a linear combination of two sinusoidal functions:

$$\vec{v}_{abc}(t) = \vec{c}_1 \cdot \cos\omega t + \vec{c}_2 \cdot \sin\omega t, \tag{4}$$

where $\vec{c}_1$, $\vec{c}_2$ are constant vectors given by the initial conditions:

$$\vec{c}_1 = \vec{v}_{abc}\Big|_{t=0}, \tag{5}$$

$$\vec{c}_2 = \frac{1}{\omega}\cdot\frac{d\vec{v}_{abc}}{dt}\Big|_{t=0}. \tag{6}$$

This means that the $\vec{v}_{abc}$ trajectory, or locus, is always contained into the plane defined by $\vec{c}_1$ and $\vec{c}_2$, as shown in Fig. 1. This figure shows the λ trajectory described by $\vec{v}_{abc}$ in the orthogonal *abc* reference frame which is within the Π–plane derived from $\vec{c}_1$ and $\vec{c}_2$. It is important to mention that $\vec{v}_{abc}$ is always within this plane irrespective of its imbalance content. The λ voltage locus can be represented in the proposed RRF which can be defined according to Fig. 2 as follows. RRF is composed by the set of unitary orthonormal row vectors $\{\vec{e}_x, \vec{e}_y, \vec{e}_o\}$, where $\{\vec{e}_x, \vec{e}_y\}$ are within the Π–plane and $\vec{e}_o$ is normal to it. Both reference frames, *abc* and RRF, are related

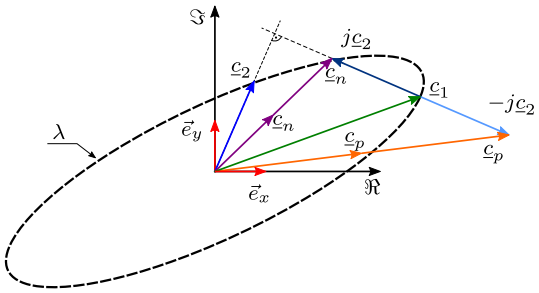

FIGURE 3. Graphical computation of $\underline{c}_p, \underline{c}_n$ given $\underline{c}_1, \underline{c}_2$ in the instant $t = 0$.

by a linear transformation

$$\vec{v}_{xyo}(t) = \left[v_x(t), v_y(t), v_0(t)\right]^T = T_R^{ext}\cdot\vec{v}_{abc}(t), \tag{7}$$

where T_R^{ext} is an orthogonal matrix defined by

$$T_R^{ext} = \begin{bmatrix}\vec{e}_x\\ \vec{e}_y\\ \vec{e}_o\end{bmatrix}. \tag{8}$$

However, note that the component $v_o(t)$ is always zero because λ is within the Π–plane and $\vec{e}_o$ is normal to it. Therefore, it is possible to consider a reduced version of the transformation just involving those components within the Π–plane:

$$\vec{v}_{xy}(t) = T_R\cdot\vec{v}_{abc}(t), \tag{9}$$

where

$$T_R = \begin{bmatrix}\vec{e}_x\\ \vec{e}_y\end{bmatrix}. \tag{10}$$

Once the voltage $\vec{v}_{abc}$ has been reduced to a two component vector $\vec{v}_{xy}$, it is possible to apply complex algebra and consider this voltage as a complex magnitude:

$$\underline{v}_{xy}(t) = \begin{bmatrix}1 & j\end{bmatrix}\vec{v}_{xy}(t) = \underline{c}_1\cdot\cos\omega t + \underline{c}_2\cdot\sin\omega t, \tag{11}$$

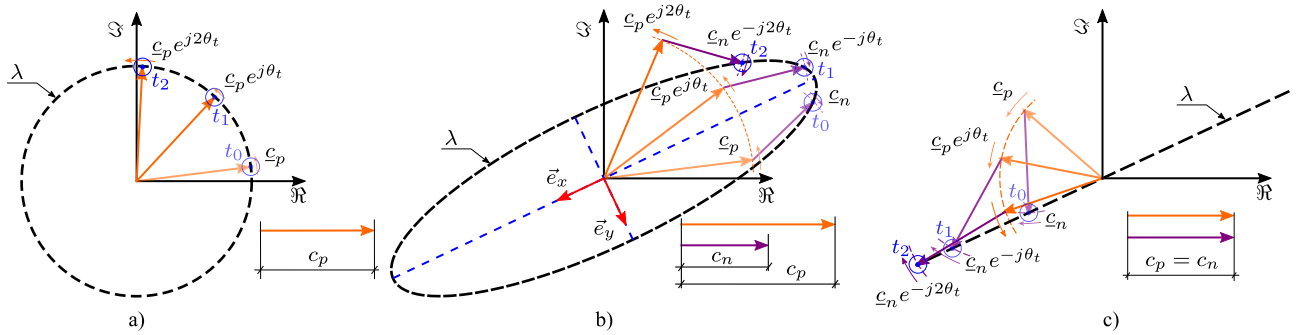

FIGURE 4. λ loci for the different classes: (a) Class I, (b) Class II, (c) Class III.

where

$$\underline{c}_1 = \begin{bmatrix} 1 & j \end{bmatrix} T_R \vec{c}_1 \qquad \underline{c}_2 = \begin{bmatrix} 1 & j \end{bmatrix} T_R \vec{c}_2. \tag{12}$$

Equation (11) can be further transformed applying Euler's identity:

$$\underline{v}_{xy}(t) = \underline{c}_p \cdot e^{j\omega t} + \underline{c}_n \cdot e^{-j\omega t}, \tag{13}$$

where

$$\underline{c}_p = \frac{\underline{c}_1 - j\,\underline{c}_2}{2} \qquad \underline{c}_n = \frac{\underline{c}_1 + j\,\underline{c}_2}{2}. \tag{14}$$

These equations can be represented in a graphical form as shown in Fig. 3, where the instant $t = 0$ is detailed. Therefore, $\underline{v}_{xy}$ can be formulated as a sum of two complex magnitudes, $\underline{c}_p$ and $\underline{c}_n$, rotating in opposite directions:

$$\underline{v}_{xy}(t) = \underline{v}^p_{xy}(t) + \underline{v}^n_{xy}(t) \qquad \begin{cases} \underline{v}^p_{xy} = \underline{c}_p \cdot e^{j\omega t} \\ \underline{v}^n_{xy} = \underline{c}_n \cdot e^{-j\omega t} \end{cases} \tag{15}$$

B. CLASSIFICATION OF λ LOCUS

This subsection establishes a classification of the possible λ loci depending on the complex vectors $\underline{c}_p$ and $\underline{c}_n$. For this purpose, it is interesting to note that (13) can be also interpreted as the parametric equation of an ellipse whose eccentricity can be computed as

$$\epsilon = \sqrt{1 - \frac{(c_p - c_n)^2}{(c_p + c_n)^2}}, \tag{16}$$

where $c_p = \left\|\underline{c}_p\right\|$ and $c_n = \left\|\underline{c}_n\right\|$. The λ locus can be classified in three different categories as summarized in Tab. 1 depending on ϵ. These different loci have been detailed in a graphical manner for three consecutive instants in Fig. 4.

TABLE 1. Classes of λ loci.

Class	Condition	Eccentricity	Locus shape
I	$c_p = 0$ or $c_n = 0$	$\epsilon = 0$	Circular
II	$c_p \neq c_n \neq 0$	$0 < \epsilon < 1$	Elliptical
III	$c_p = c_n$	$\epsilon = 1$	Linear

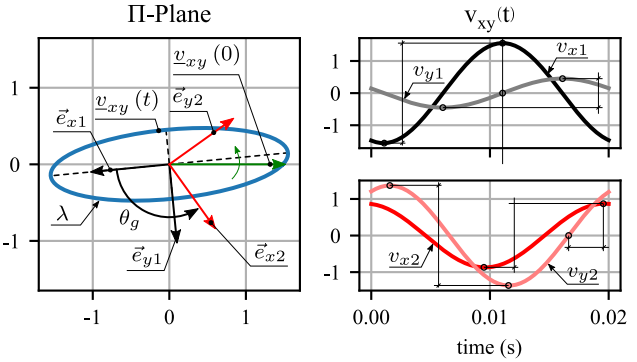

FIGURE 5. Class II λ trajectory and its components with two different reference frames within the Π–plane. Black lines for RRF axes, red lines for alternative axes.

Class I and Class III refer to two degenerated cases where the eccentricity is zero and one respectively. The λ locus associated to Class I is a circumference, which occurs when c_p or c_n equals zero. The λ locus of Class III, where c_p and c_n are equal, defines a trajectory following a line. Finally, Class II refers to the general case where λ is an ellipse with a eccentricity $0 < \epsilon < 1$. Note that this trajectory can be defined using any two orthonormal axis within the Π–plane. It is proposed, however, to take advantage of the two symmetry axis associated to the ellipsoidal λ locus, namely the semi-minor and semi-major axes. The benefits of using this reference frame, which is a contribution with respect to [25], are illustrated in Fig. 5 and are summarized as follows:

- The components $v_x(t)$ and $v_y(t)$ are delayed $\pi/2$.
- The amplitudes of $v_x(t)$ and $v_y(t)$, A_x and A_y respectively, are equal to the length of the of semi-major and semi-minor axes, which can be formulated as:

$$A_x = c_p + c_n \;;\; A_y = c_p - c_n. \tag{17}$$

- The eccentricity ϵ is related to the amplitudes A_x and A_y. Substituting (17) into (16), the ratio of amplitudes k can be expressed as:

$$k = \frac{A_y}{A_x} = \sqrt{1 - \epsilon^2}. \tag{18}$$

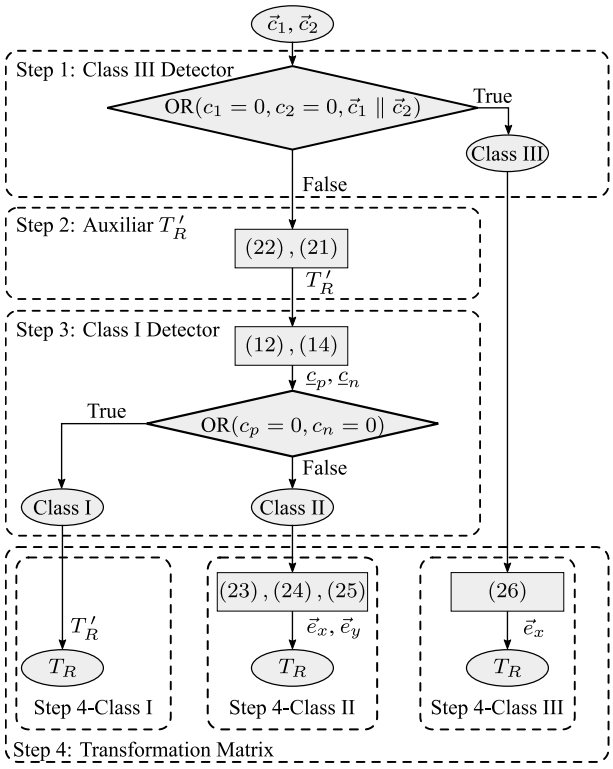

FIGURE 6. Flowchart of the RRF transformation matrix computation.

- Using the above properties, it is possible to formulate the λ trajectory using just one of the components:

$$\underline{v}_{xy}(\omega t) = v_x(\omega t) + j\, k\, v_x\left(\omega t + \frac{\pi}{2}\right). \tag{19}$$

C. COMPUTATION OF THE TRANSFORMATION MATRIX

This section is devoted to compute the transformation matrix required to convert from the *abc* phase domain to the proposed RRF. It must be noted that the transformation matrix is computed depending on the λ locus class discussed in the previous subsection. For this reason, it is required to follow a number of steps as illustrated in the flowchart depicted in Fig. 6:

- Step 0. Obtain the constant vectors $\vec{c}_1$ and $\vec{c}_2$ of the magnitude to be transformed:

$$\vec{c}_1 = \sqrt{2}\begin{bmatrix} V_a\cos(\theta_a) \\ V_b\cos(\theta_b) \\ V_c\cos(\theta_c) \end{bmatrix},$$
$$\vec{c}_2 = -\sqrt{2}\begin{bmatrix} V_a\sin(\theta_a) \\ V_b\sin(\theta_b) \\ V_c\sin(\theta_c) \end{bmatrix}. \tag{20}$$

- Step 1. Check if the λ locus is linear (Class III). This happens in case of $c_p = c_n$. Resorting to (14), one of the following conditions are fulfilled:
  - Vectors $\vec{c}_1$ and $\vec{c}_2$ are parallel. This implies that $\underline{c}_1$ and $\underline{c}_2$ are proportional, i.e., $\underline{c}_2 = k\,\underline{c}_1$, with $k \neq 0$.
  - One of the vectors $\vec{c}_1$ or $\vec{c}_2$ is null. This implies that $\underline{c}_1 = 0$ or $\underline{c}_2 = 0$.

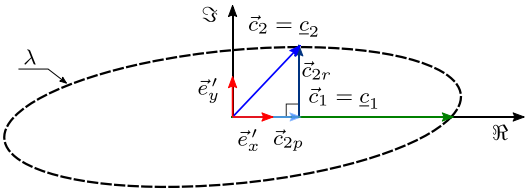

FIGURE 7. Computation of the auxiliary transformation matrix T'_R.

If the locus is linear, continue to Step 4-Class III. Otherwise, continue to Step 2.

- Step 2. Compute an auxiliary transformation matrix T'_R from vectors $\vec{c}_1$ and $\vec{c}_2$ given the fact that these vectors are within the Π–plane:

$$T'_R = \begin{bmatrix} \vec{e}'_x \\ \vec{e}'_y \end{bmatrix} = \begin{bmatrix} \dfrac{\vec{c}_1}{\|\vec{c}_1\|} \\ \dfrac{\vec{c}_{2r}}{\|\vec{c}_{2r}\|} \end{bmatrix}. \tag{21}$$

Note that $\vec{c}_{2r}$ is the rejection of $\vec{c}_2$ into $\vec{c}_1$ which, according to Fig. 7, can be computed as:

$$\vec{c}_{2r} = \vec{c}_2 - \vec{c}_{2p} = \vec{c}_2 - \frac{\vec{c}_2 \cdot \vec{c}_1}{\|\vec{c}_1\|^2} \cdot \vec{c}_1, \tag{22}$$

where $\vec{c}_{2p}$ is the projection of $\vec{c}_2$ into $\vec{c}_1$.

- Step 3. Check if the λ locus is a circumference (Class I). For this purpose, $\underline{c}_1$, $\underline{c}_2$ and $\underline{c}_p$, $\underline{c}_n$ are computed by applying (12) and (14) respectively. The λ locus is a circumference if either c_p or c_n equals zero. In this case, continue to Step 4-Class I. Otherwise the λ locus is elliptical and continue to Step 4-Class II.
- Step 4-Class I. In this case, the λ locus is a circumference as shown in Fig. 4.a. Therefore, any orthogonal set of unitary vectors within the Π–plane will have a similar performance. The λ locus projection on any orthogonal axis will produce two sinusoidal components with the same amplitude but delayed $\pi/2$ each other. This is shown in Fig. 8 where the effect of choosing different reference sets is depicted. It is clearly noticed that the unique difference refers to the initial phase of the two signals. Therefore, T'_R is chosen as the transformation matrix.
- Step 4-Class II. As previously mentioned, in this case the semi-major and semi-minor axis, symmetry axis associated to the ellipsoidal λ locus, are used as the reference frame. Note that the semi-major axis is always in the bisector of $\underline{c}_p$ and $\underline{c}_n$, as shown in Fig. 9, which is computed as the square root of their corresponding unitary vectors:

$$\underline{e}_x = \left(\frac{\underline{c}_p}{\|\underline{c}_p\|} \cdot \frac{\underline{c}_n}{\|\underline{c}_n\|}\right)^{1/2}. \tag{23}$$

In this way, $\underline{e}_x$ is an unitary vector whose angle will be the average angle of $\underline{c}_p$ and $\underline{c}_n$ and, consequently,

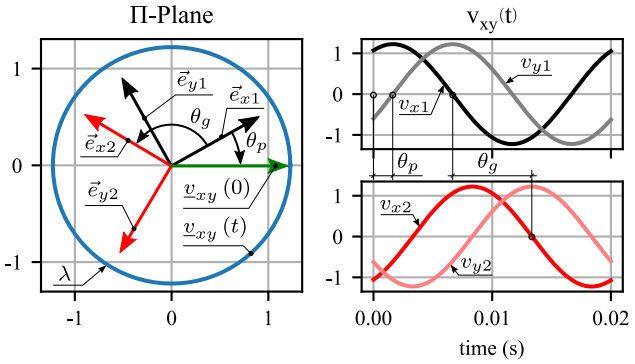

FIGURE 8. Class I λ trajectory and its components with two different reference frames within the Π–plane. Black lines for RRF axes, red lines for alternative axes.

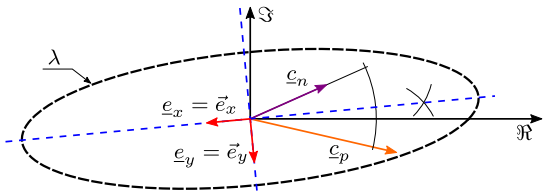

FIGURE 9. Graphical computation of direction of mayor and minor axes given $\underline{c}_p$, $\underline{c}_n$.

oriented with the semi-major axis. The semi-minor axis, $\underline{e}_y$, is oriented as follows:

$$\underline{e}_y = j\,\underline{e}_x\,. \tag{24}$$

Returning to the vector space, directions $\vec{e}_x$ and $\vec{e}_y$ can be computed as follows:

$$\vec{e}_x = T_R'^{T}\begin{bmatrix}\Re\{\underline{e}_x\}\\ \Im\{\underline{e}_x\}\end{bmatrix};\quad \vec{e}_y = T_R'^{T}\begin{bmatrix}\Re\{\underline{e}_y\}\\ \Im\{\underline{e}_y\}\end{bmatrix}, \tag{25}$$

defining the transformation matrices T_R^{ext} and T_R in (8) and (10) respectively.

- Step 4-Class III. In this case, λ locus is linear and only $\vec{e}_x$ is needed to define the transformation matrix. This can be considered a particular case of class II ($\epsilon = 1$). Using the axis $\vec{e}_x$ computed by:

$$\vec{e}_x = \frac{\vec{c}_i}{\|\vec{c}_i\|}, \tag{26}$$

where $\vec{c}_i$ is the non-null vector among $\vec{c}_1$ and $\vec{c}_2$. Selecting another axis $\vec{e}_y$ such as $\vec{e}_y \perp \vec{e}_x$, the component associated with the semi-minor axis, A_y, is null ($k = 0$) and the magnitude is just represented by $\underline{v}_x$ as shown in Fig. 10. Note that the selection of any other arbitrary axis within the Π–plane will have two non-null components.

III. POWER THEORY

This section is devoted to define the power magnitudes in the proposed RRF. For this purpose, the instantaneous active

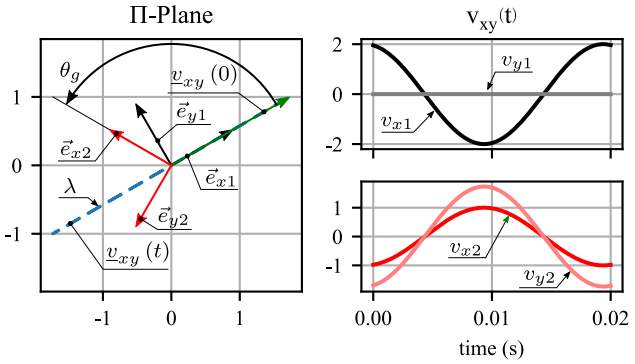

FIGURE 10. Class III λ trajectory and its components with two different reference frames within the Π–plane. Black lines for RRF axes, red lines for alternative axes.

and reactive powers formulated in the phase domain are considered [29]:

$$p\,(t) = \vec{v}_{abc}\,(t)^T \cdot \vec{i}_{abc}\,(t)\,, \tag{27}$$

and

$$q\,(t) = \|\vec{q}_{abc}\,(t)\|, \tag{28}$$

where $\vec{q}_{abc}\,(t)$ is defined using the cross product

$$\vec{q}_{abc}\,(t) = \vec{v}_{abc}\,(t) \times \vec{i}_{abc}\,(t)\,. \tag{29}$$

These power terms can be computed using voltages and currents expressed in the RRF. However, it has to be considered that voltages and currents may not have the same Π–plane in a general case. Therefore, if the voltage Π–plane is used for the transformation, the current may have a non-null o component. For this reason, it is required to use the vector formulation rather than the complex algebra for obtaining the different power terms. Considering that the matrix T_R^{ext} is orthogonal, the RRF transformation is power invariant:

$$p(t) = \vec{v}_{xyo}\,(t)^T \cdot \vec{i}_{xyo}\,(t)\,, \tag{30}$$

$$q\,(t) = \|\vec{q}_{xyo}\| = \|\vec{v}_{xyo}\,(t) \times \vec{i}_{xyo}\,(t)\,\|. \tag{31}$$

Note that if $\vec{v}_o$ is null, the active and reactive power terms can be simplified as follows:

$$p\,(t) = v_x \cdot i_x + v_y \cdot i_y, \tag{32}$$

$$\vec{q}_{xyo}\,(t) = \begin{bmatrix} v_y \cdot i_o \\ -v_x \cdot i_o \\ v_y \cdot i_x - v_x \cdot i_y \end{bmatrix}. \tag{33}$$

The active power and each of the reactive power components can be divided into constant and variable terms as they depend on the product of two sinusoidal magnitudes,

$$p\,(t) = \overline{p} + \tilde{p}\,(t), \tag{34}$$

$$q_k\,(t) = \overline{q}_k + \tilde{q}_k(t) \quad k = x, y, o, \tag{35}$$

where $\overline{p}$ and $\overline{q}_k$ refer to the constant terms and $\tilde{p}$ and $\tilde{q}_k$ to the oscillatory ones. This power formulation is greatly simplified in case of a common Π–plane for the voltage and current loci. In this case, the current i_o is null and the reactive power has

only one component in the o axis. Therefore, it is possible to formulate the active and reactive powers as:

$$\begin{bmatrix} p \\ q \end{bmatrix} = \begin{bmatrix} v_x & v_y \\ v_y & -v_x \end{bmatrix} \cdot \begin{bmatrix} i_x \\ i_y \end{bmatrix}. \tag{36}$$

Note that this formulation is similar to that formulated by Akagi in [11], but with the advantage that it can be used in a straightforward manner even with voltages and currents with zero–sequence components. Similarly, (36) can be adapted to a complex formulation as proposed in [16], but extending its application to voltages and currents including zero–sequence components:

$$p(t) + j\,q(t) = \underline{v}_{xy}(t) \cdot \underline{i}^{\star}_{xy}(t), \tag{37}$$

where * means conjugate.

IV. CASE STUDY

This section applies the proposed RRF to the particular three–phase four–wire system shown in Fig. 11 for illustration purposes. The phase voltages of the unbalanced ideal source are:

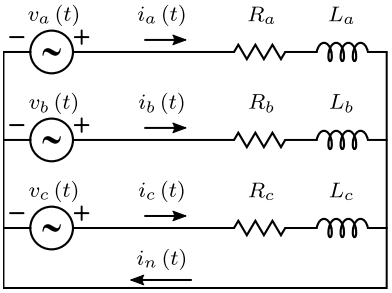

FIGURE 11. Three–phase four–wire case study.

$$\begin{cases} v_a\,(t) = 224.4\,\cos\left(\omega\,t - 2.6012\right)\,\text{V} \\ v_b\,(t) = 243.4\,\cos\left(\omega\,t + 1.2490\right)\,\text{V} \\ v_c\,(t) = 154.0\,\cos\left(\omega\,t\right)\,\text{V}, \end{cases} \tag{38}$$

where the amplitudes and the phase angle of each phase are totally different as depicted in Fig. 12.a. This three–phase voltage source is connected to the loads detailed in Tab. 2. Particularly, two cases are analyzed to evidence the performance of the RRF transformation and the related power formulation in case of voltages and currents with different and equal Π–plane respectively. In the first simulation, an unbalanced three–phase load is used, with the phase c impedance lower than the corresponding values for phases a and b, while the second one connects a balanced three–phase load.

The transformation to the RRF can be computed following the flowchart detailed in Fig. 6 to the supply voltages. The intermediate results obtained in each step are presented in Tab. 3 and the final transformation matrix is

$$T_R^{ext} = \frac{1}{3}\begin{bmatrix} -2 & 2 & 1 \\ -1 & -2 & 2 \\ 2 & 1 & 2 \end{bmatrix}.$$

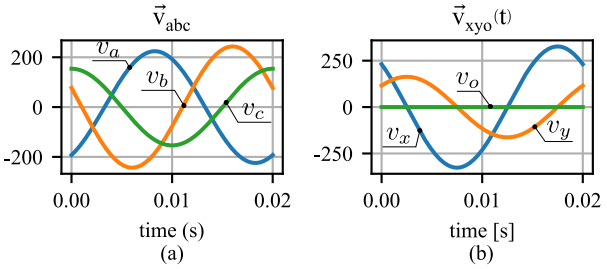

FIGURE 12. Unbalanced load case. a) Voltages in the *abc* frame. b) Voltages in the RRF.

TABLE 2. Load parameters for unbalanced and balanced case studies.

Case Study	Parameters
Unbalanced	$R_a = R_b = 120\,\Omega$, $R_c = 84\,\Omega$ $L_a = L_b = 1.2$ H, $L_c = 0.84$ H
Balanced	$R_a = R_b = R_c = 120\,\Omega$ $L_a = L_b = L_c = 1.2$ H

TABLE 3. Intermediate results for obtaining the transformation matrix in the proposed case study.

Step	Parameters
1	$\vec{c}_1 = [-192.42, 76.98, 154]^T$ V $\vec{c}_2 = [115.45, -230.91, 0]^T$ V $c_1 \neq 0, c_2 \neq 0, \vec{c}_1 \nparallel \vec{c}_2 \Rightarrow$ It Is not Class III
2	$\vec{c}_{2p} = [115.42, -46.18, -92.38]^T$ V $\vec{c}_{2r} = [0.026, -184, 73, 92.38]^T$ V $\vec{e}'_x = [-0.745, 0.298, 0.596]^T$ $\vec{e}'_y = [0.00012, -0.894, 0.447]^T$
3	$\underline{c}_1 = 258.20 + 0\,j$ V $\underline{c}_2 = -154.88 + 206.54\,j$ V $\underline{c}_p = 232.37 + 77.44\,j$ V $\underline{c}_n = 25.83 - 77.44\,j$ V $c_p = 244.93$ V $c_n = 81.64$ V $\epsilon = 0.866$ $c_p \cdot c_n \neq 0, 0 < \epsilon < 1 \Rightarrow$ It is not Class I
4-II	$\underline{e}_x = 0.894 - 0.447\,j$ $\underline{e}_y = 0.447 + 0.894\,j$ $\vec{e}_x = \frac{1}{3}[-2, 2, 1]^T$ $\vec{e}_y = \frac{1}{3}[-1, -2, 2]^T$ $\vec{e}_o = \frac{1}{3}[2, 1, 2]^T$

A. UNBALANCED LOAD

The load current in *abc* coordinates is illustrated in Fig. 13.a where a high current circulation through the neutral wire i_n is observed due to the load and voltage imbalance. The voltages and currents in the RRF are shown in Fig. 12.b and Fig. 13.b respectively after applying the transformation matrix to the

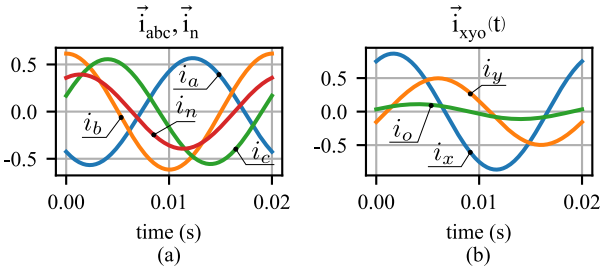

FIGURE 13. Unbalanced load case. a) Currents in the *abc* frame including the neutral current. b) Currents in the RRF.

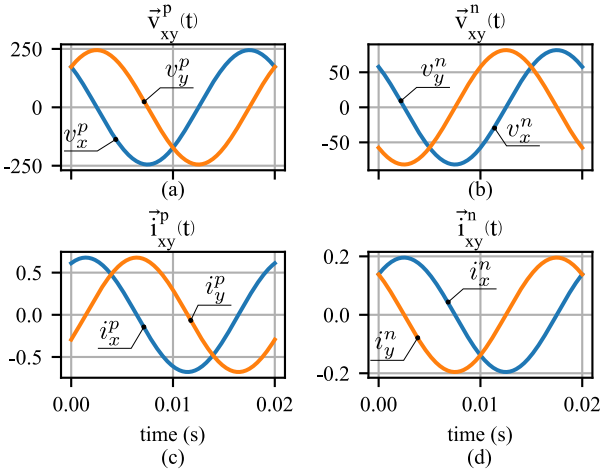

FIGURE 14. Unbalanced load case. Decomposition of $\underline{v}_{xy}$ and $\underline{i}_{xy}$ in rotating complex vectors. a) Voltage clockwise components. b) Voltage counterclockwise components. c) Current clockwise components. d) Current counterclockwise components.

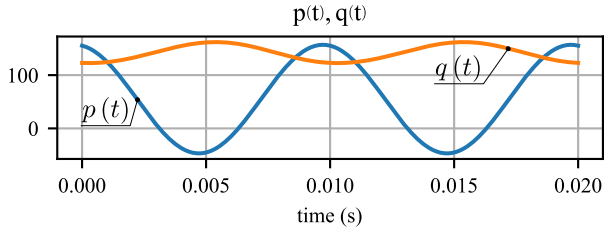

FIGURE 15. Unbalanced load case. Instantaneous active and reactive power.

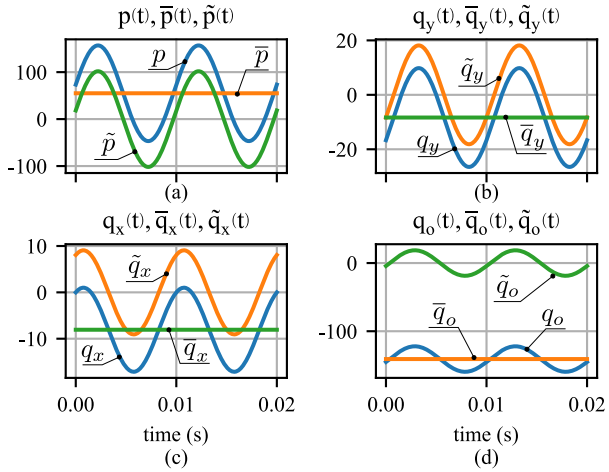

FIGURE 16. Unbalanced load case. Decomposition of active power and reactive power components into constant and variable terms. (a) Active power. (b) Reactive power in *y* axis. c) Reactive power in *x* axis. d) Reactive power in *o* axis.

abc magnitudes. Note that v_o is null because the voltage is within the computed Π–plane. In addition, v_y lags v_x a phase angle equal to $\pi/2$, one of the properties of using the semi-major and semi-minor axis of the λ locus previously analyzed in subsection II-B. Other interesting property of the proposed RRF transformation is the ratio of v_x over v_y. This is related to the λ locus eccentricity, ϵ, which equals to 0.866. The analysis of the currents reveals that i_o is not zero since the load is unbalanced and the Π–plane has been computed using the voltages rather than the currents. In this sense, the currents have their own Π–plane which may be different from the voltage one.

Once the voltages and currents are formulated in the RRF, it is possible to consider their *xy* components as complex magnitudes which can be represented as a sum of two complex vectors with constant amplitude rotating in opposite directions as presented in subsection II-B. Fig. 14 shows the projections of these components on the RRF orthonormal axes. It can be observed that each component has the same amplitude and they are delayed $\pi/2$, one of the properties derived from the axes orientation in the RRF for circular locus. In addition, this figure illustrates the direction of the rotation of these complex magnitudes which can be derived from the relative lagging between the represented projections.

Note that v^p_x and i^p_x lead with respect to v^p_x and i^p_x respectively, meaning that the complex vectors $\vec{v}^p$ and $\vec{i}^p$ rotate clockwise. Conversely, v^n_x and i^n_x lag with respect to v^n_x and i^n_x respectively because the complex vectors $\vec{v}^n$ and $\vec{i}^n$ have a counterclockwise rotation.

Finally, the instantaneous active and reactive power components, shown in Fig. 15, are computed from the transformed RRF voltages and currents applying the power theory summarized in Section III. With this regard, it is important to highlight that the current is not within the same voltage Π–plane and, therefore, its *o* component has to be considered. Consequently, the reactive power has to be computed after obtaining the different terms detailed in (33) and represented in Fig. 16. This figure also shows the constant and variable terms which are present in the active and the reactive power components.

B. BALANCED LOAD

In spite of the balanced character of the load, the current is unbalanced due to the supply voltage. In fact, the neutral current is non-null due to the voltage zero–sequence component. The effect of a balanced load can be seen in the transformed RRF currents which are in the same Π–plane than the voltage. As a result, i_o is null as shown in Fig. 17. Therefore, the computation of the active and reactive powers can be done

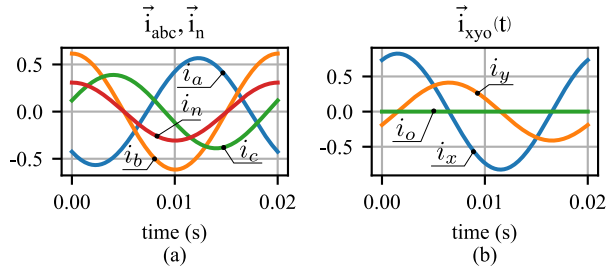

FIGURE 17. Balanced load case. a) Currents in the *abc* frame including the neutral current for balanced load. b) Currents in the RRF for balanced load.

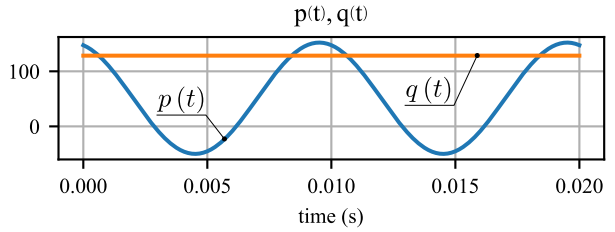

FIGURE 18. Balanced load case. Instantaneous active and reactive power for balanced load.

directly using (37) with the results shown in Fig. 18. In this sense, it is important to highlight that the reactive power computation has been done in a straightforward manner using complex algebra in a case where voltages and currents have zero–sequence components. Therefore, and in the case of a common Π–plane, the proposed RRF transformation allows to define a power theory similar to the ones defined in [11] and [16], but with voltages and currents including also zero–sequence components.

V. EXPERIMENTAL VALIDATION

This section describes a first experimental validation of the proposed RRF transformation to evidence its suitability for real-time applications. For this purpose, it has been followed a Controller Hardware-in-the-Loop (C-HIL) testing approach [30]. The three–phase circuit represented in Fig. 6 is considered as the *plant* while the RRF transformation takes over the role of the *controller* to be tested as shown in Fig. 19. This three–phase circuit is simulated in real-time using a Typhoon HIL 402 platform with a time step 0.5 μs. The simulated three–phase voltage and current, $v_{abc}(t)$ and $i_{abc,n}(t)$, are transformed from digital to analog signals using the available analog output ports. Conversely, the RRF transformation detailed in Fig. 6 is embedded into a TMS320F28335 Delfino Digital Signal Processor (DSP) from Texas Instruments. The measured analog signals are transformed into digital ones using the corresponding DSP analog input ports with a sampling frequency of 5 kHz. The computed RRF magnitudes, $v_{xyo}(t)$ and $i_{xyo}(t)$, are converted to digital 10 kHz PWM signals due to the absence of analog output ports in this DSP model. Finally, these PWM signals are captured using a Yokogawa DL850 oscilloscope with a 500 Hz low-pass input filter which eliminates the PWM high-frequency components.

TABLE 4. Simulated and experimental results.

Parameter	Simulation results (V, A, rad)	Experimental results (V, A, rad)	Error (%, rad)
V_a	158.70	159.07	0.23401
V_b	172.13	172.75	0.36122
V_c	108.87	109.09	0.20264
V_x	230.94	231.44	0.21732
V_y	115.47	115.96	0.42382
θ_a	-2.601	-2.597	0.00389
θ_b	1.249	1.251	0.00211
θ_x	0.785	0.786	0.00039
θ_y	-0.785	-0.779	0.00617
I_a	0.401	0.403	0.34751
I_b	0.435	0.437	0.38357
I_c	0.393	0.394	0.14883
I_x	0.612	0.615	0.39534
I_y	0.352	0.354	0.63971
I_o	0.079	0.078	-0.58470
θ_a	2.419	2.423	0.00389
θ_b	-0.014	-0.011	0.00242
θ_c	-1.263	-1.264	-0.00113
θ_x	-0.523	-0.520	0.00247
θ_y	-1.889	-1.883	0.00684
θ_o	-1.263	-1.272	-0.00891

The case study with the unbalanced load detailed in subsection IV.A has been considered for this experimental validation. The comparison of simulated and experimental results is detailed in Tab. 4 for voltages and currents in *abc* frame and RRF, where it has been considered the phase *c* voltage as the system reference. This table also shows the error between the simulated and experimental results, being considered a relative error (%) in the case of RMS magnitudes and an absolute error for phase angles (rad). Note that in the case of the voltages, the largest errors are 0.42 % and 0.00617 rad for RMS values and phases respectively. This can be also visually verified comparing the signals of Fig. 20, which shows the experimental phase voltages *abc* (top plot) and the experimental RRF transformed voltages *xyo* (bottom plot), with respect to the simulation voltages in Fig. 12. It is interesting to note that v_o is also null in the experimental validation which clearly indicates that the RRF transformation has been successfully applied in the DSP with a correct identification of the voltage Π–plane. In addition, Fig. 20 and Tab. 4 show that the phase angle difference between v_x and v_y is $\pi/2$, one of the RRF properties derived from using the semi-major and semi-minor axes of the voltage locus as reference frame.

Figure 21 shows the experimental currents in *abc* frame (top plot) and RRF (bottom plot). The largest errors for current RMS magnitudes and phase angles are 0.64 % and 0.00891 rad respectively according to Tab. 4. Although these errors are slightly higher than those obtained for voltages, they are quite small being possible to claim that experimental

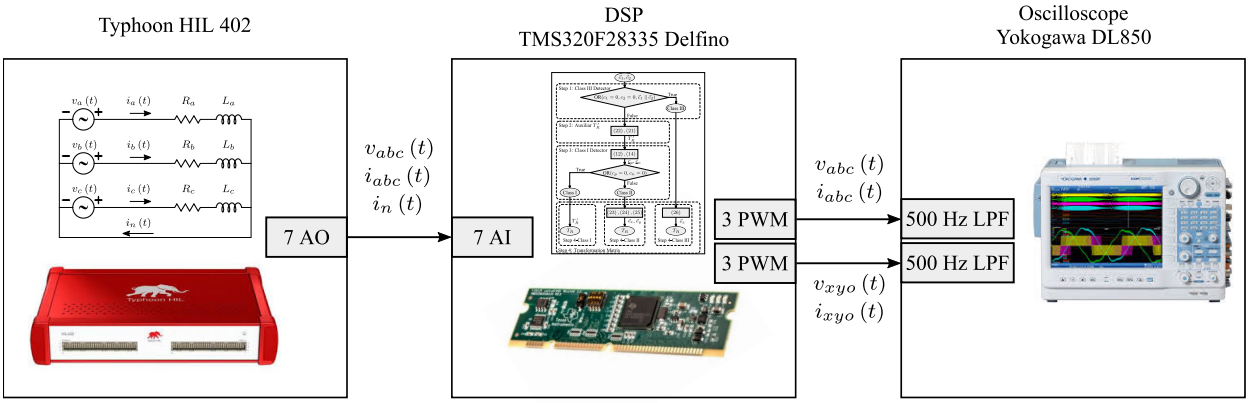

FIGURE 19. Experimental validation of the RRF transformation following a C-HIL approach.

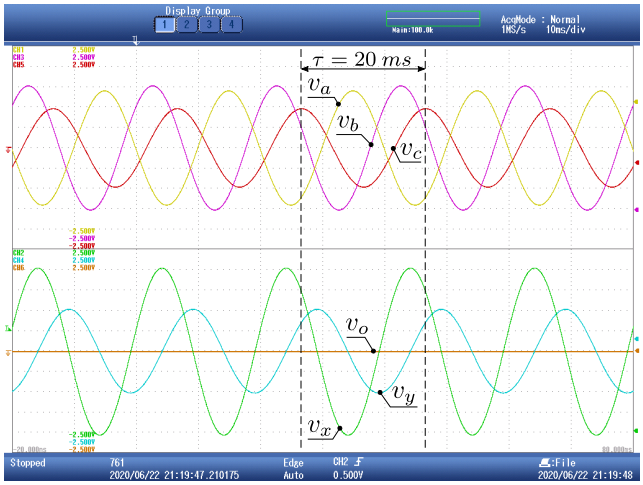

FIGURE 20. Experimental voltages: ***abc*** frame (top plot) and RRF frame (bottom plot). Scale 1 V: 160 V.

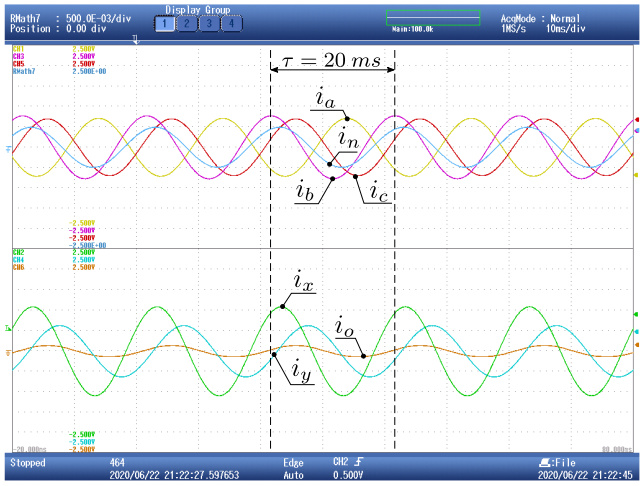

FIGURE 21. Experimental currents: ***abc*** frame (top plot) and RRF frame (bottom plot). Scale 1.25 V: 1 A.

currents match the simulated ones. This similarity can be also verified by comparing Fig. 21 and Fig. 13. Note that i_o is not null because the current is not in the same voltage Π–plane.

VI. CONCLUSION

This paper has presented a transformation for sinusoidal three–phase and four–wire systems named Reduced Reference Frame (RRF). For this purpose, it has been considered that the three–phase magnitude can be represented as a space vector $\vec{v}_{abc}$ describing a trajectory in an orthogonal *abc* space where each axis is associated to a phase magnitude. The proposed transformation to the RRF allows to represent this trajectory within a plane, namely the Π–plane. Therefore, the voltage is reduced to just two components which are referred to a set of orthogonal axis in the Π–plane. The paper has proposed a general classification of the possible trajectories (circular, ellipsoidal and linear loci) depending on the characteristics of the transformed three–phase magnitude. It has been demonstrated that the linear and circular loci are two degenerated cases of the more general ellipsoidal trajectory. In this sense, it is important to highlight that this paper has proposed the semi-major and semi-minor axes of the trajectory as the reference frame taking advantage of some symmetry properties. Additionally, a step-by-step methodology for computing the transformation matrix depending on each of the possible trajectory classes is included. Once the magnitudes are transformed into the RRF, it has been defined a power theory in a similar way than in the original *abc* domain. The paper has included two case studies to detail all the steps to compute the RRF transformation and also the application of the power theory in this new reference frame. Finally, and in spite of this paper is mainly devoted to the RRF fundamentals, an experimental validation has been also included to evidence the suitability of applying the RRF transform for real-time applications.

This novel approach may constitute an alternative method to the classical transformations provided by Fortescue, Park and Clarke and applied so far in different electrical engineering fields. The application of the proposed RRF transformation may overcome the well–known limitations of those classical tools in case of three–phase and four–wire systems. For this reason, future work will explore possible applications of the RRF

transform in circuit theory, electrical machines and power electronics.

ACKNOWLEDGMENT

The authors would like to thank to Andrei Mihai Gross his support on the experimental validation of the RRF transformation included in this paper.

REFERENCES

[1] F. Milano, *Power System Modelling and Scripting*, vol. 54. Berlin, Germany: Springer, 2010.

[2] P. C. Krause, O. Wasynczuk, S. D. Sudhoff, S. Pekarek, and Institute of Electrical and Electronics Engineers, *Analysis of Electric Machinery and Drive Systems*. Hoboken, NJ, USA: Wiley, 2002.

[3] A. Yazdani and R. Iravani, *Voltage-Sourced Converters in Power Systems: Modeling, Control, and Applications*. Hoboken, NJ, USA: Wiley, 2010.

[4] C. L. Fortescue, "Method of symmetrical co-ordinates applied to the solution of polyphase networks," *Trans. Amer. Inst. Electr. Eng.*, vol. 37, no. 2, pp. 1027–1140, Jul. 1918.

[5] B.-I. Jung, H.-S. Choi, Y.-S. Cho, and D.-C. Chung, "Analysis of the unbalanced fault in three-phase flux-coupling type SFCL using the symmetrical coordinate method," *IEEE Trans. Appl. Supercond.*, vol. 22, no. 3, Jun. 2012, Art. no. 5601305.

[6] R. H. Park, "Two-reaction theory of synchronous machines generalized method of analysis-Part I," *Trans. Amer. Inst. Elect. Eng.*, vol. 48, no. 3, pp. 716–727, Jul. 1929.

[7] W. C. Duesterhoeft, M. W. Schulz, and E. Clarke, "Determination of instantaneous currents and voltages by means of alpha, beta, and zero components," *Trans. Amer. Inst. Electr. Engineers*, vol. 70, no. 2, pp. 1248–1255, Jul. 1951.

[8] B. K. Bose, *Modern Power Electronics and AC Drives*. Upper Saddle River, NJ, USA: Prentice-Hall, 2002.

[9] K. Ogata, *Modern Control Engineering*. Upper Saddle River, NJ, USA: Prentice-Hall, 2002.

[10] S. Bifaretti, P. Zanchetta, and E. Lavopa, "Comparison of two three-phase PLL systems for more electric aircraft converters," *IEEE Trans. Power Electron.*, vol. 29, no. 12, pp. 6810–6820, Dec. 2014.

[11] H. Akagi, Y. Kanazawa, and A. Nabae, "Instantaneous reactive power compensators comprising switching devices without energy storage components," *IEEE Trans. Ind. Appl.*, vols. IA–20, no. 3, pp. 625–630, May 1984.

[12] H. Akagi, A. Nabae, and S. Atoh, "Control strategy of active power filters using multiple voltage-source PWM converters," *IEEE Trans. Ind. Appl.*, vol. IA-22, no. 3, pp. 460–465, May 1986.

[13] P. Rodriguez, A. V. Timbus, R. Teodorescu, M. Liserre, and F. Blaabjerg, "Flexible active power control of distributed power generation systems during grid faults," *IEEE Trans. Ind. Electron.*, vol. 54, no. 5, pp. 2583–2592, Oct. 2007.

[14] L. Feola, R. Langella, and A. Testa, "On the effects of unbalances, harmonics and interharmonics on PLL systems," *IEEE Trans. Instrum. Meas.*, vol. 62, no. 9, pp. 2399–2409, Sep. 2013.

[15] M. E. Meral and D. Çelík, "A comprehensive survey on control strategies of distributed generation power systems under normal and abnormal conditions," *Annu. Rev. Control*, vol. 47, pp. 112–132, 2019.

[16] A. Ferrero and G. Superti-Furga, "A new approach to the definition of power components in three-phase systems under nonsinusoidal conditions," *IEEE Trans. Instrum. Meas.*, vol. 40, no. 3, pp. 568–577, Jun. 1991.

[17] J. L. Willems, "A new interpretation of the akagi-nabae power components for nonsinusoidal three-phase situations," *IEEE Trans. Instrum. Meas.*, vol. 41, no. 4, pp. 523–527, 1992.

[18] H. Akagi, E. H. Watanabe, and M. Aredes, *Instantaneous Power Theory and Applications to Power Conditioning*. Hoboken, NJ, USA: Wiley, 2006.

[19] H. Akagi, S. Ogasawara, and H. Kim, "The theory of instantaneous power in three-phase four-wire systems: A comprehensive approach," in *Proc. Conf. Rec. IEEE Ind. Appl. Conf. 34th IAS Annu. Meeting*, vol. 1, Oct. 1999, pp. 431–439.

[20] M. Aredes and E. H. Watanabe, "New control algorithms for series and shunt three-phase four-wire active power filters," *IEEE Trans. Power Del.*, vol. 10, no. 3, pp. 1649–1656, Jul. 1995.

[21] M. Godoy Simões, F. Harirchi, and M. Babakmehr, "Survey on time-domain power theories and their applications for renewable energy integration in smart-grids," *IET Smart Grid*, vol. 2, no. 4, pp. 491–503, Dec. 2019. [Online]. Available: http://www.ietdl.org

[22] G. Tan, J. Cheng, and X. Sun, "Tan-sun coordinate transformation system theory and applications for three-phase unbalanced power systems," *IEEE Trans. Power Electron.*, vol. 32, no. 9, pp. 7352–7380, Sep. 2017. [Online]. Available: http://ieeexplore.ieee.org/document/7676330/

[23] P. Granjon and G. S. L. Phua, "Estimation of geometric properties of three-component signals for system monitoring," *Mech. Syst. Signal Process.*, vol. 97, pp. 95–111, Dec. 2017, doi: 10.1016/j.ymssp.2017.04.002.

[24] V. Choqueuse, P. Granjon, A. Belouchrani, F. Auger, and M. Benbouzid, "Monitoring of three-phase signals based on singular-value decomposition," *IEEE Trans. Smart Grid*, vol. 10, no. 6, pp. 6156–6166, Nov. 2019.

[25] A. A. Montanari and A. M. Gole, "Enhanced instantaneous power theory for control of grid connected voltage sourced converters under unbalanced conditions," *IEEE Trans. Power Electron.*, vol. 32, no. 8, pp. 6652–6660, Aug. 2017. [Online]. Available: https://ieeexplore.ieee.org/abstract/document/7740053

[26] C. J. O'Rourke, M. M. Qasim, M. R. Overlin, and J. L. Kirtley, "A geometric interpretation of reference frames and transformations: Dq0, clarke, and park," *IEEE Trans. Energy Convers.*, vol. 34, no. 4, pp. 2070–2083, Dec. 2019.

[27] T. A. Lipo, "A Cartesian vector approach to reference frame theory of AC machines," in *Proc. Int. Conf. Electr. Mach.*, Laussane, Switzerland, 1984, pp. 1–4.

[28] P. A. Tipler and G. Mosca, *Physics for Scientists Engineers*, 6th ed. New York, NY, USA: W.H. Freeman, 2004.

[29] F. Zheng Peng and J.-S. Lai, "Generalized instantaneous reactive power theory for three-phase power systems," *IEEE Trans. Instrum. Meas.*, vol. 45, no. 1, pp. 293–297, 1996.

[30] P. Kotsampopoulos, D. Lagos, N. Hatziargyriou, M. O. Faruque, G. Lauss, O. Nzimako, P. Forsyth, M. Steurer, F. Ponci, A. Monti, V. Dinavahi, and K. Strunz, "A benchmark system for Hardware-in-the-Loop testing of distributed energy resources," *IEEE Power Energy Technol. Syst. J.*, vol. 5, no. 3, pp. 94–103, Sep. 2018.

FRANCISCO CASADO-MACHADO (Graduate Student Member, IEEE) was born in Seville, Spain, in 1990. He received the degree in mechanical engineering, the degree in electrical engineering, and the M.Sc. degree in electric energy systems from the University of Seville, in 2014, 2015, and 2018, respectively, where he is currently pursuing the Ph.D. degree. He was a Power System Engineer at Abengoa, Seville, from 2014 to 2018. Since 2018, he has been with the Department of Electrical Engineering, University of Seville, as a Research Assistant. His research interest includes power system modeling, analysis, and control.

JOSE L. MARTINEZ-RAMOS (Senior Member, IEEE) was born in Dos Hermanas, Spain, in 1964. He received the Ph.D. degree in electrical engineering from the University of Seville, Seville, Spain, in 1994. Since 1990, he has been with the Department of Electrical Engineering, University of Seville, where he is currently a Full Professor. His research interests include active and reactive power optimization, power system planning, analysis, and control, and electricity markets.

MANUEL BARRAGÁN-VILLAREJO was born in Marmolejo, Spain, in 1984. He received the degree and the Ph.D. degree in electrical engineering from the University of Seville, Seville, Spain, in 2008 and 2014, respectively. Since 2008, he has been with the Department of Electrical Engineering, University of Seville, where he is currently an Assistant Professor. His primary research interests include exploitation and control of power converter for smart grid management and grid integration of renewable energy resources.

JOSÉ MARÍA MAZA-ORTEGA (Member, IEEE) received the degree and the Ph.D. degree from the University of Seville, Spain, in 1996 and 2001, respectively. Since 1997, he has been with the Department of Electrical Engineering, University of Seville, where he is currently an Associate Professor. His primary research interests include power quality, harmonic filters, and the integration of renewable energies and power electronics.

JOSÉ A. ROSENDO-MACÍAS (Senior Member, IEEE) was born in Carmona, Spain. He received the degree in electrical engineering and the Ph.D. degree from the University of Seville, Spain. Since 1992, he has been with the Department of Electrical Engineering, University of Seville, where he is currently a Professor. His primary research interest include dynamic state estimation, digital signal processing, digital relaying, and distribution reliability.